Experimental Search for Two Photon Exchange in *ep* Elastic Scattering

B. A. Raue

Florida International University
Miami, FL, U.S.A.

Two photon exchange (TPE) has been proposed as the primary source of the discrepancy between Rosenbluth and polarization-transfer methods of determining the electric-to-magnetic form-factor ratio of the proton. A direct measurement of the TPE contribution to elastic scattering is necessary to verify this hypothesis. In this proceeding I will briefly review the motivation for the TPE search, discuss how one experimentally obtains the real part of the TPE amplitude, and present some of the details of setting up such an experiment. I will also present some very preliminary results from Jefferson Lab and discuss what is expected to be measured in the very near future.

1. Introduction

Elastic scattering of electrons on protons is one of the simplest processes studied in nuclear physics. Under the assumption of single-photon exchange, known as the Born Approximation, the elastic cross section is given by

$$\left(\frac{d\sigma}{d\Omega}\right)_{lab} = \left(\frac{d\sigma}{d\Omega}\right)_{Mott} \frac{1}{\epsilon\,(1+\tau)} \left[\epsilon G_E^2(Q^2) + \tau G_M^2(Q^2)\right], \tag{1}$$

where the Mott cross section describes scattering from a point-like particle and $G_E^2(Q^2)$ and $G_M^2(Q^2)$ are the Sachs electric and magnetic form factors. The other variables are kinematic quantities that are defined in the appendix. The electromagnetic form factors, simplistically, describe the distribution of charge and current within the proton and are discussed extensively by Professor Tomasi elsewhere in these proceedings.

One way to determine the form factors is through what is known as a Rosenbluth separation.[1] In a Rosenbluth separation the cross section is measured as a function of ϵ at fixed Q^2. A linear fit of the reduced cross section, $\sigma_{red} = \left[\epsilon G_E^2(Q^2) + \tau G_M^2(Q^2)\right]$, then has a slope of G_E^2 and a y-intercept of τG_M^2. Two examples of Rosenbluth separations[2] are shown in Fig. 1 at $Q^2 = 2.75$ and 4.25 GeV^2. This was the predominant method of extracting the form factors for many years and the database for the elastic-scattering cross section is quite extensive. (See Ref.[3] and references therein.)

One can also determine the ratio G_E/G_M through polarization transfer measurements.[4–7] For example, in the reaction of $\vec{e} + p \rightarrow e + \vec{p}$, one can measure the transverse (P_T) and longitudinal (P_L) polarizations of the outgoing protons. The ratio of the form factors is then given by

$$\frac{G_E}{G_M} = -\frac{P_T}{P_L}\frac{(E+E')}{2m_p}\tan\frac{\theta}{2}. \tag{2}$$

This technique was first used at MIT Bates[8] followed by a series of measurements at Jefferson Lab[9–11,13–17] and Mainz.[12] One can also extract the form-factor ratio using a polarized electron beam on a polarized proton target.[19,20]

Fig. 2 shows the ratio $\mu_p G_E/G_M$ (where μ_p is the magnetic moment of the proton) as measured by the two methods. There is an obvious discrepancy between the Rosenbluth points (hollow) and the polarization results (solid) that grows with Q^2.

The most prevalent explanation that has been put forth to resolve this discrepancy is that two photon exchange (TPE) contributes to the elastic cross section at level larger than previously expected. Fig. 3 shows the various diagrams that contribute to elastic scattering. It is the Born diagram that we are interested in for determining the form factors. Diagrams (a)-(d) and (g) and (h) are generally accounted for by "standard" radiative corrections[24,25] while diagrams (e) and (f) are the two-photon exchange terms, which are ignored in the standard corrections. The motivation for ignoring the TPE diagrams has been the expectation that they must only contribute on the order of α^2 (α being the fine structure constant) while the other terms contribute to order α. However, since the intermediate state in the TPE diagrams can be not only a proton but any accessible baryon resonance or a continuum state, it is not hard to imagine that these diagrams may well sum up to a significant contribution.

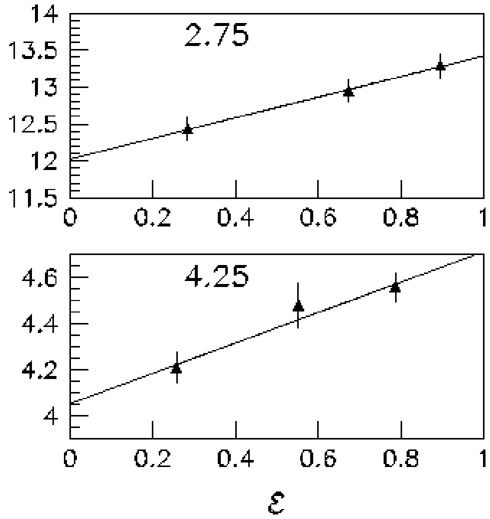

Fig. 1. Typical Rosenbluth separations[2] showing the reduced cross section ($\times 10^3$) vs. ϵ for Q^2 = 2.75 and 4.25 GeV^2, as indicated.

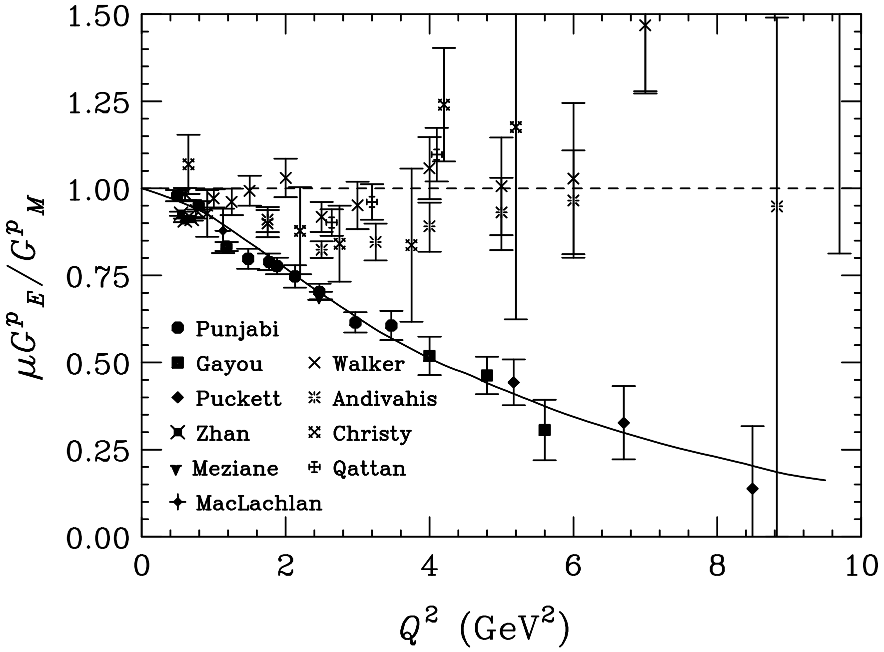

Fig. 2. Proton form factor ratio $\mu_p G_E^p/G_M^p$ from polarization-transfer measurements (filled symbols) of Puckett,[16] Punjabi and Jones,[9] Gayou[13] Zhan,[17] Meziane,[11] and MacLachlan,[14] as well as from Rosenbluth measurements of Walker,[21] Andivahis,[22] Christy,[2] and Qattan.[23] The solid curve is a global fit of polarization results from Ref.[18]

It is the very fact that there are so many possible intermediate states–mostly with unknown photo-couplings–that make a reliable calculation of the TPE correction so difficult. Nonetheless, many such calculations* have been recently done, several of which do a remarkable job of reconciling the form-factor discrepancy. For example, the Hadronic Intermediate State model of Blunden, Melnitchouk, and Tjon[27] has been used to correct the Rosenbluth data as shown in Fig. 4. Further corrections have come even closer to reconciling the form-factor discrepancy.[3]

*For an excellent review of our current knowledge of TPE, including a summary of TPE calculations, see Ref.[26]

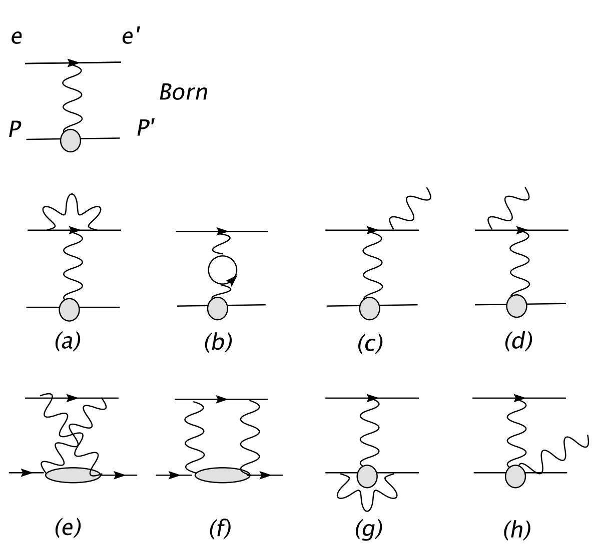

Fig. 3. Feynman diagrams for elastic electron-proton scattering, including the 1st-order QED radiative corrections. Diagrams (e) and (f) show the two-photon exchange e terms, where the intermediate state can be an unexcited proton, a baryon resonance or a continuum of hadrons.

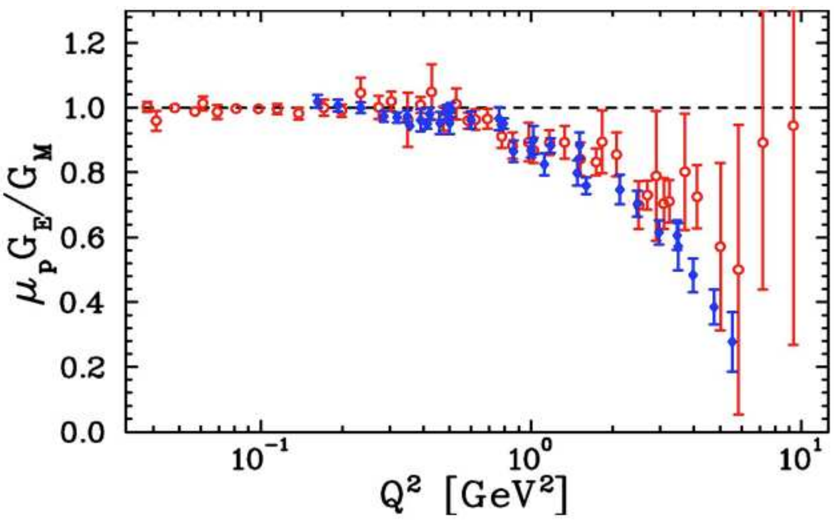

Fig. 4. Comparison of form-factor ratios for polarization transfer data (filled diamonds) and Rosenbluth data corrected for TPE effects (open circles) using the HIS calculation.[27]

2. Direct Measurement of TPE

Though TPE is the most likely explanation for the form-factor discrepancy, a direct measure of the TPE amplitude is essential. A direct model-independent measurement of the TPE correction can be achieved experimentally by finding the ratio of the positron-proton to electron-proton elastic cross sections.

The amplitude of elastic ep-scattering with an accuracy of α_{em}^2 can be written as

$$A_{total} = e_e e_p A_{Born} + e_e^2 e_p A_{e.br.} + e_e e_p^2 A_{p.br.} + e_e^2 e_p^2 A_{2\gamma}, \tag{3}$$

where the amplitudes $A_{Born}, A_{e.br.}, A_{p.br.}$ and $A_{2\gamma}$ respectively describe one-photon exchange, electron bremsstrahlung, proton bremsstrahlung and two-photon exchange. Note that radiative corrections such as vertex corrections and vacuum polarization do not contribute to the charge asymmetry and are therefore not included here. Squaring the above amplitude and keeping the corrections up to order α_{em} that have odd powers of electron charge, we have

$$|A_{ep\to ep}|^2_{odd} = e_e^2 e_p^2 [|A_{Born}|^2 + e_e e_p A_{Born} 2Re(A^*_{2\gamma}) + e_e e_p 2Re(A_{e.br.} A^*_{p.br.})], \tag{4}$$

where the notation Re is used for the real part of the amplitude.

Corrections that have an even power of lepton charge, including the largest correction from electron bremsstrahlung, do not lead to any charge asymmetry. The last term in the above expression describes interference between electron and proton bremsstrahlung. Its infrared divergence exactly cancels the corresponding infrared divergence of the term $A_{Born}Re(A^*_{2\gamma})$. This interference effect for the standard kinematics of elastic ep-scattering experiments is dominated by soft-photon emission and results in a factorizable correction already included in the standard approach to radiative corrections.[24]

Therefore, after correcting for the interference between electron and proton bremsstrahlung, one can isolate the TPE term by taking the ratio of positron- to electron-proton cross sections:

$$\sigma(e^{\pm}) = \sigma_{Born}(1 \mp \delta_{2\gamma}), \tag{5}$$

$$R_{2\gamma} = \frac{\sigma(e^+)}{\sigma(e^-)} \approx 1 - 2\delta_{2\gamma}, \tag{6}$$

where $\delta_{2\gamma}$ is the two photon exchange correction factor. Obviously, in the absence of TPE effects, R is equal to one.

Since $\delta_{2\gamma}$ is expected to be of order 0.01, one needs to measure $R_{2\gamma}$ with to an uncertainty of no more that $\sim$ 1%. To do this with separate cross section measurements is very difficult. One must control factors such as the lepton flux, the target thickness, and the beam energy precisely, as well as maintaining a high degree of certainty on detector acceptance. Experiments can typically do no better than few percent for the systematic uncertainty.

2.1. *Previous Experimental Work*

Though it is difficult to measure $R_{2\gamma}$ precisely, there were several experiments in the 1960's to do just that.[†] The first experiment took place in 1962 at the Stanford Mark III Linac (a predecessor to SLAC).[29] This was followed by a series of seven other experiments through 1968. Fig. 5 shows these data plotted vs. ϵ. These data span $0.01 < Q^2 < 5.0$ GeV^2 and the entire ϵ range. However, the size of the uncertainties and the relative lack of low ϵ make it impossible to discern any significant deviation from unity. In Ref.,[28] a linear fit to the data for $Q^2 < 2.0$ GeV^2 did find a large non-zero slope (0.057±0.018) but there is almost certainly some Q^2 dependence that has not been disentangled from the ϵ dependence.

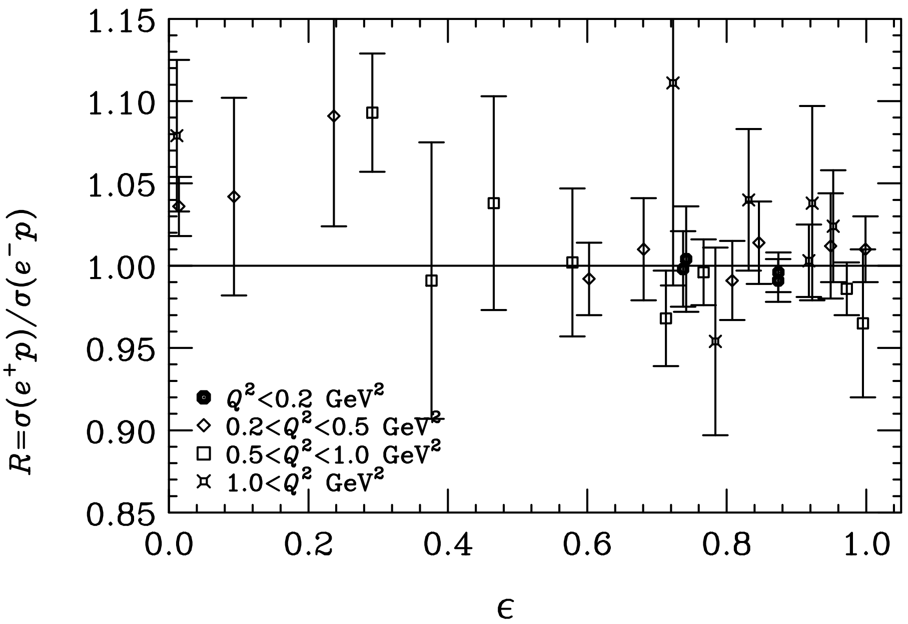

Fig. 5. Previous world data on $R_{2\gamma}$.[28] Data for different Q^2 ranges are indicated by different symbols as shown on the figure.

At the time of these measurements, the large uncertainties on $R_{2\gamma}$ were enough to convince people that TPE was negligible, at least relative to the typical size of uncertainties on the cross section measurements available. Clearly, given the size of the form-factor discrepancy that now exists, that is no longer the case and more precise measurements of $R_{2\gamma}$ are now required.

[†] See Ref.[28] for a summary of the early electron-positron ratio measurements.

3. The CLAS TPE Experiment

The CLAS TPE experiment[30] will measure $R_{2\gamma}$ for $Q^2 \leq 3.0$ GeV^2 and nearly the entire range of ϵ with small uncertainties. Systematic uncertainties of $\sim$ 1% will be achieved by using a novel technique of simultaneous measurements of electron and positron elastic scattering yields. In this way, factors that contribute to systematic uncertainties in cross section measurements–such as incident particle flux, target thickness, and detector acceptances–will largely cancel out.

3.1. *Experimental Details*

The experiment took place at the Thomas Jefferson National Accelerator Facility (Jefferson Lab) in Newport News, Virginia, U.S.A. At the heart of Jefferson Lab is the CEBAF superconducting electron accelerator capable of achieving continuous, high intensity beams with energies of almost 6 GeV. The beam can be simultaneously delivered to each of the three experimental halls–A, B, or C.

For this experiment, the CEBAF Large Acceptance Spectrometer (CLAS)[31] in Hall B was used. CLAS (shown in Fig. 6) is a nearly 4π detector. The magnetic field is provided by six superconducting coils, which produce an approximately toroidal field in the azimuthal direction around the beam axis. The regions between the six magnet cryostats are instrumented with identical detector packages called sectors. Each sector consists of three regions of drift chambers (R1, R2, and R3) to determine the trajectories of charged particles, Cherenkov Counters (CC) for electron identification, Scintillation Counters (SC) for time of flight information, and Electromagnetic Calorimeters for electron identification and neutral particle detection. The R2 drift chambers are in the region of the magnetic field and provide tracking that is then used to determine particle momenta with $\delta p/p \sim 0.6\%$ In this experiment, the CC's were not used and the EC's were only used as a cross check.

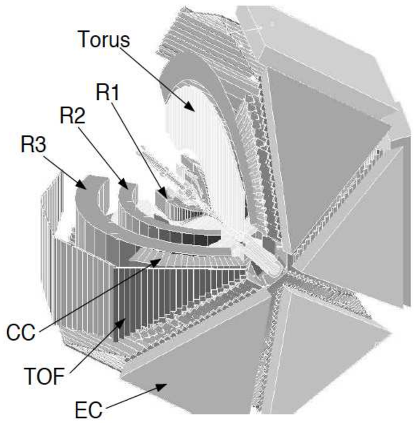

Fig. 6. Three dimensional view of CLAS showing various components as described in the text. In this view, the beam enters the picture from the upper left corner.

In order to produce simultaneous positron and electron beams, the electron beam was first incident upon a gold radiator foil to produce a photon beam through Bremsstrahlung. The Hall B tagger magnet[32] was then used to divert the electrons into an underground beam dump. The photon beam then struck a gold converter to produce e^+/e^- pairs. The beams then entered a three-dipole chicane to separate the lepton beams from the photon beam. The photon beam was stopped by a tungsten block, while the leptons were recombined into a single beam at the third dipole before proceeding to a liquid hydrogen target at the center of CLAS. Fig. 7 shows the layout of the beamline.

A feasibility test run of the experiment was conducted in 2006 in which most of the elements shown in Fig. 7 were in place. A primary electron-beam energy of 3.3 GeV and $\sim$ 100 nA was used to produce a beam current $|I| \sim 20$ pA (each charge) of tertiary beam current with $0.5 \leq E \leq 3.3$ GeV on an 18-cm-long LH^2 target. While the run's primary goal was to study backgrounds and count rates, data useful extracting $R_{2\gamma}$ were taken for about $1\frac{1}{2}$ days. The CLAS torus polarity was flipped periodically, which cancels out lepton acceptance affects. The data acquisition was triggered on events with TOF hits in opposite CLAS sectors with one hit being at $\theta < 40°$.

3.2. *Data Analysis*

In this analysis we were faced with a number of issues that are uncommon to the majority of CLAS experiments. For example, the energy of the incident lepton is not known and the standard methods of lepton identification cannot be applied because we do

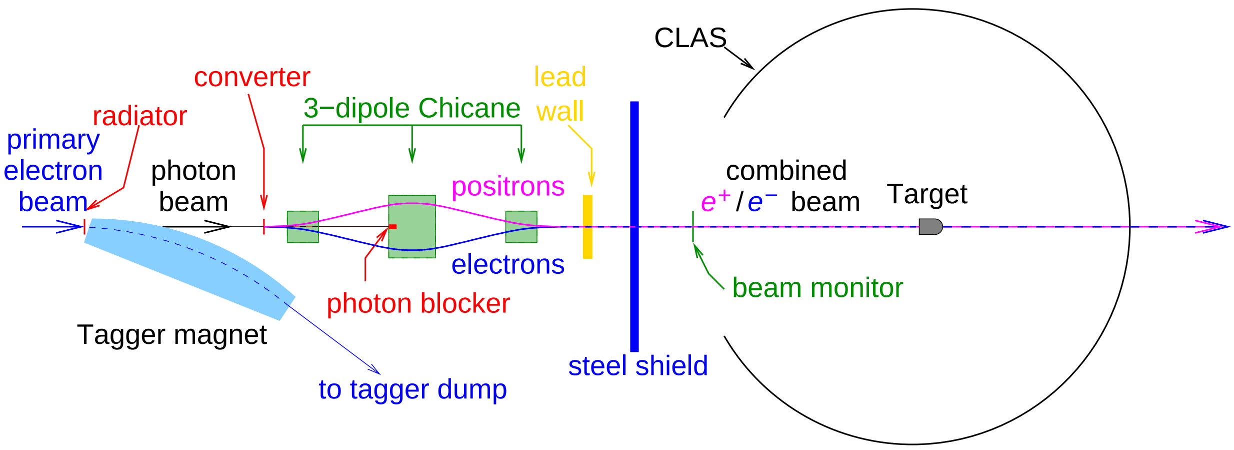

Fig. 7. Beamline sketch for the CLAS TPE experiment.

not have CC or EC information. The solution to this is to require the detection of the protons along with the leptons and exploit elastic-scattering kinematics and other cuts to identify events of interest and to match the detector acceptances for the two types of events (electron-proton and positron-proton). A description of the important analysis techniques is given below.

3.2.1. *Elastic Event Identification*

The first step in event identification was to isolate the events with only two particles in the final state and require that these particles were in opposite sectors. A cut was also placed on the charge of these final state tracks, and only events with positive/negative or positive/positive charge combination were kept. In order to determine which particle was the proton and which was the positron in positive/positive events, a threshold of $\beta > 0.9$ was imposed to decide which particle was the positron. A $\beta > 0.9$ would require $p_p > 1.94$ GeV, which is well above our elastic acceptance limit of $p_p < 1.8$ GeV. For positive/positive events that did not subsequently satisfy the additional cuts listed below, we swapped the identities of the two positive particles and checked to see if they then satisfied the additional cuts. They did not.

The additional cuts included bad paddle removal, event vertex cuts, and range limitations applied to six individual kinematic variables that correspond to the elastic scattering interaction. These are summarized in the list below. As will be shown, these cuts were correlated in that any single cut has minimal effect when all of the other cuts are applied. This lead to a very clean elastic event distributions with minimal background contamination. Figs. 8-11 show some of the cut variables. Unless otherwise indicated, they show the combined data for both torus polarities.

(1) **Bad paddle removal.** As CLAS has aged, some of the TOF photomultiplier tubes (PMT) have deteriorated in performance and no longer give reliable information. Events that register hits in these paddles have been removed from the analysis.
(2) ***Z*-vertex.** Using the CLAS drift chambers to reconstruct the particle trajectories, the event origin along the beamline (z-vertex) can be identified. A cut was placed on z-vertex to ensure that events came from the LH^2 target.
(3) Azimuthal opening angle (co-planarity). Since there are only two particles in the final state, these events must be co-planar. Fig. 8 shows the azimuthal-angle difference between events before and after all other cuts.
(4) **Transverse momentum.** Because the beam travels along the z-axis, conservation of momentum requires the total transverse momentum of the final elastic scattering products to be zero. Therefore, good elastic events will result in a transverse momentum peaked near zero as shown in Fig. 9.
(5) **Beam energy difference.** Because we measured the energies and 3-momenta for both particles in the final state, our kinematics are over constrained. This allows us to reconstruct the unknown energy of the incident lepton (tertiary beam energy) in two different ways. Equation 7 finds the incident energy using the scattered lepton and proton angles, whereas equation 8 calculates this value from the total momentum along the z direction.

$$E^{angles}_{beam} = m_p\left(\cot\frac{\theta_{e^\pm}}{2}\cot\theta_p - 1\right) \quad (7)$$

$$E^{mom.}_{beam} = p_{e^\pm}\cos\theta_{e^\pm} + p_p\cos\theta_p \quad (8)$$

Assuming perfect momentum and angle reconstruction, these two quantities should be the same resulting in $\Delta E_{beam} \equiv E^{angles}_{beam} - E^{mom.}_{beam} = 0$. The ΔE_{beam} distribution is shown in Fig. 10. The 7 to 22 MeV shift in the centroids from zero is due to

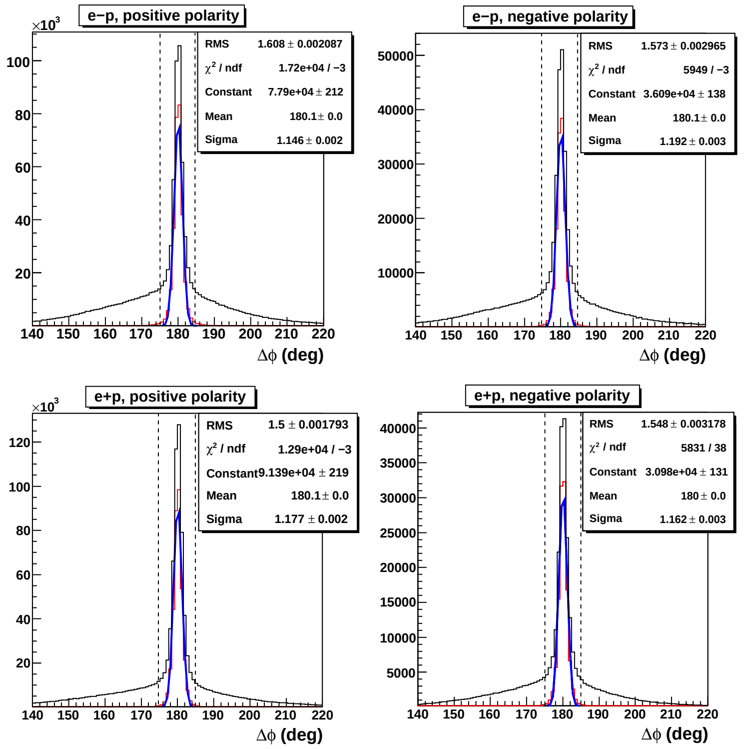

Fig. 8. Angle between lepton and proton ($\Delta\phi$) distributions for event type and torus polarity as indicated. The black histogram is the data before all cuts except the opposite sector cut. The red histogram is after all other cuts and the blue curve is its Gaussian fit. The dashed lines show the applied cut.

energy losses, which will reduce the value of $E_{beam}^{mom.}$. Events that fall outside of this cut include those in which the final state has three or more particles with one undetected. Note that in later calculations that depend on beam energy (Q^2, W, ϵ), we

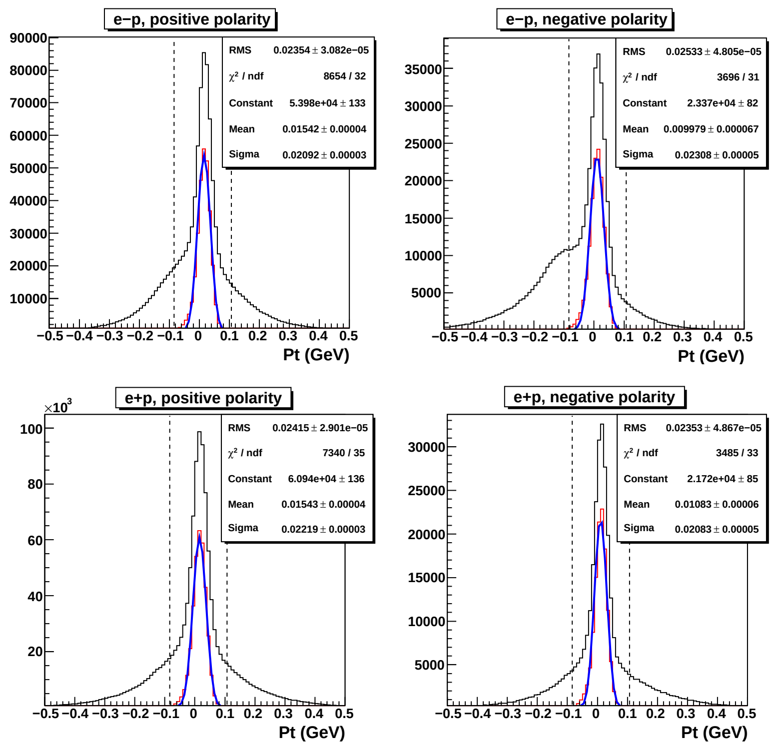

Fig. 9. Reconstructed transverse momentum distributions for event type and torus polarity as indicated. The black histogram is the data before all cuts except the opposite sector cut. The red histogram is after all other cuts and the blue curve is its Gaussian fit. The dashed lines show the applied cut.

have used E_{beam}^{angles}.

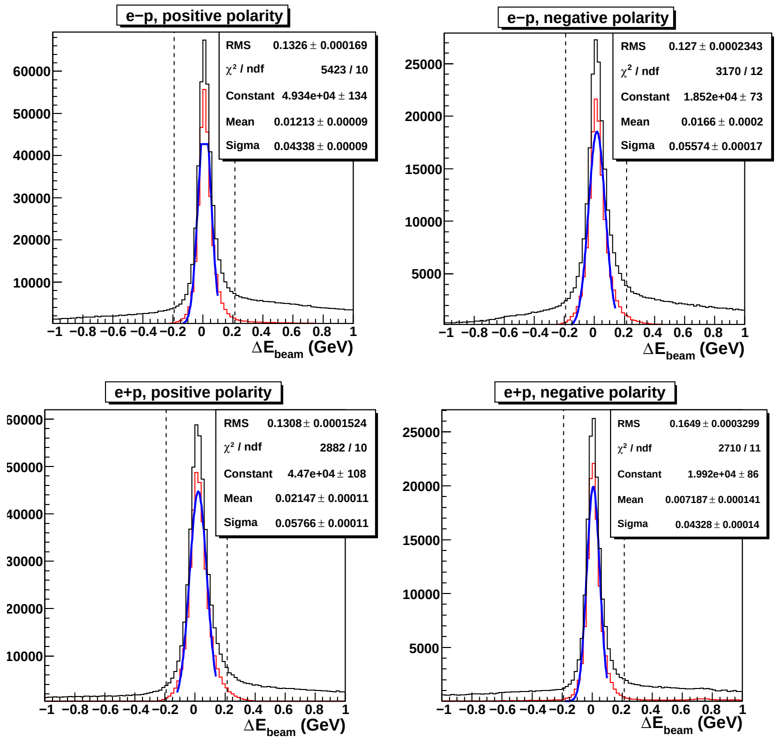

Fig. 10. ΔE_{beam} for event type and torus polarity as indicated. Black histogram is the data before all cuts except the opposite sector cut. The red histogram is after all other cuts and the blue curve is its Gaussian fit. The dashed lines show the applied cut.

(6) **Beam polar angle.** The reconstructed incident lepton ($\vec{p}_l = \vec{p}_{l'} + \vec{p}_{p'}$) was required to travel along the z axis. Any large deviations may be due to inelastic events, mis-reconstructed scattered particles, or multiple-scattered final particles. To discard these background events, the beam polar angle–from the reconstructed three-momenta of the detected particles–was required to be $\theta_{beam} < 5°$. The beam polar angle distribution is presented in Fig. 11. This cut also has the effect of removing events with a missing particle so it is largely redundant to the beam energy difference cut and the transverse momentum cut.

(7) **Distance of closest approach between lepton and proton candidates.** The distance of closest approach in this context is defined as the distance that two tracks (lepton and proton) come closest to one another. The shortest distance is found using an algorithm that draws a line perpendicular to both tracks and calculates the length of this line and a cut is placed on this distance to ensure the two tracks come from the same event.

(8) **Fiducial cuts.** Fiducial cuts are used to select the region of CLAS with uniform acceptance.

The cuts for above items 3,4,5,7 and 8 were determined by fitting a Gaussian to the peak of the combined distribution for that variable of both event types and torus polarities and setting the cut to $\pm 4\sigma$.

The cleanliness of the final data sample after these cuts were applied is show in Fig. 12, which is a $W = \sqrt{m_p + 2m_p\nu - Q^2}$ distribution for one of our bins in ϵ. The peak is at the proton mass–as expected–and is completely without any hint of non-elastic background.

The distribution of events in Q^2 vs. ϵ after all cuts is shown in Fig. 13. The green boxes in the figure show the bins used for the final analysis, while the pink boxes show the binning used in our systematic uncertainty analysis. The final results cover a single Q^2 bin ($0.125 \le Q^2 \le 0.400$ GeV^2 with $\langle Q^2 \rangle = 0.206$ GeV^2) and seven bins in ϵ ($0.830 \le \epsilon \le 0.943$) such that we have similar statistical uncertainties in each ϵ bin. This allows direct comparison to previously existing data.

3.2.2. *Acceptance Corrections*

Clearly, the detector acceptances for electrons and positrons for a given kinematic bin are going to be different because one bends away from the beam line while the other bends toward the beam line in the CLAS magnetic field. We have accounted for this acceptance difference by using an acceptance-matching algorithm. This “swimming” algorithm calculates the trajectory

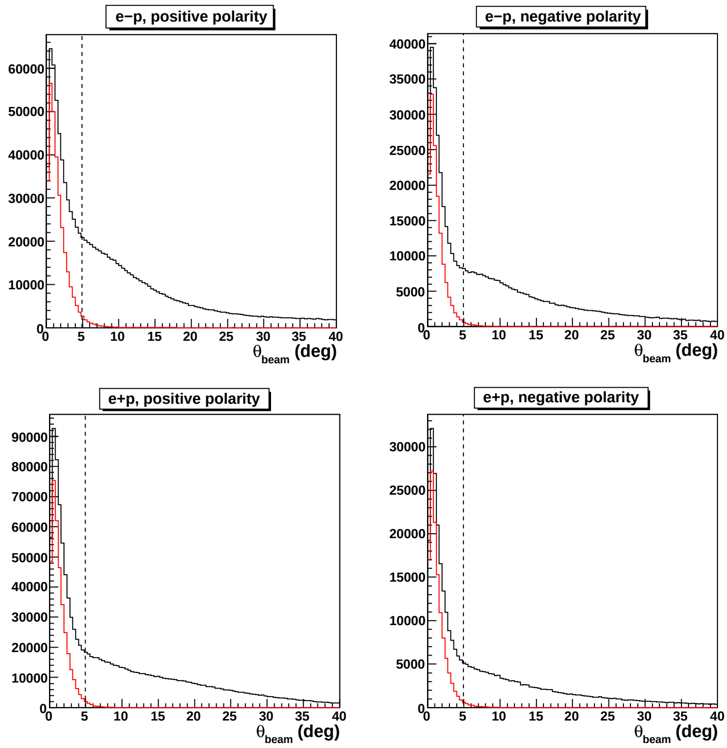

Fig. 11. Reconstructed polar angle of the beam for event type and torus polarity as indicated. Black histogram is the data before all cuts except the opposite sector cut and the red histogram is after all other cuts. The dashed lines show the applied cut.

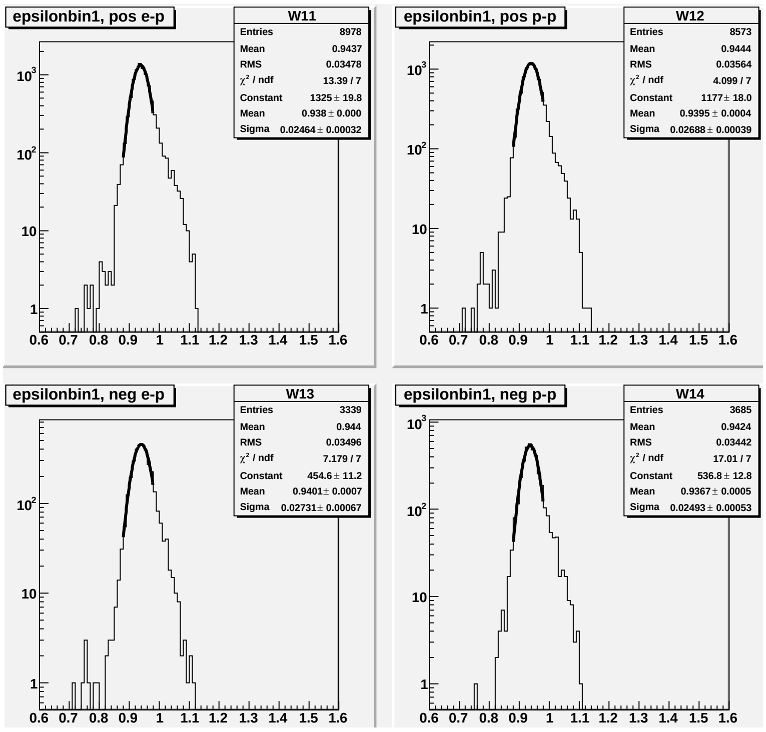

Fig. 12. Top two panels show the W distributions (in GeV) for positive torus polarity electron (left) and positron (right) events for $0.820 \leq \epsilon \leq 0.840$ and $\langle Q^2 \rangle = 0.206\ \mathrm{GeV}^2$ with all cuts applied. The bottom two panels show the same for negative torus polarity events. A Gaussian fit is included in the region around the peak.

of particles through the CLAS detector system and magnetic field. The acceptance matching was done by taking each event, say an $e^- p$ event, generating the conjugate lepton with the same kinematic quantities (p and θ), and swimming the hypothetical

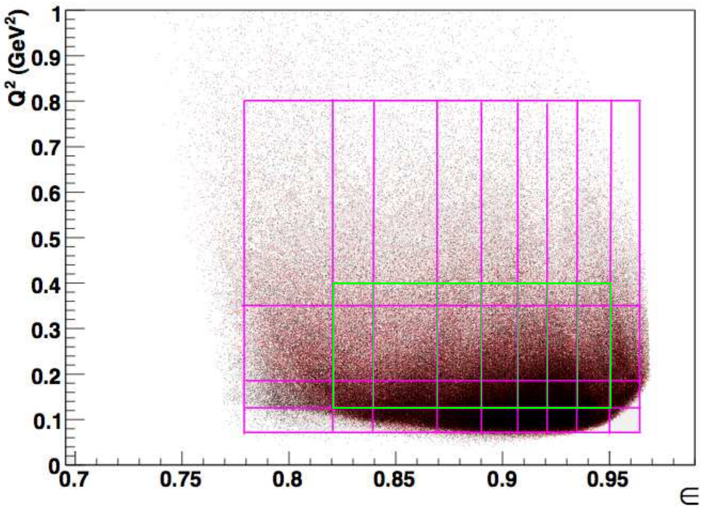

Fig. 13. Binning scheme, shown for negative polarity for electrons (black) and positrons (red). The green boxes show the binning for the final data and the pink boxes show the fine bins used in the systematics studies.

lepton through CLAS–an e^+ in this case. If the conjugate event remains in the CLAS acceptance, the original event is kept. If the conjugate event falls outside of the CLAS acceptance (either outside fiducial cuts or hits a bad paddle), the event is discarded, thus ensuring that the two types of events have the same kinematic acceptances.

The remaining differences between torus settings can be removed in the ratio cross sections as follows:

$$\begin{aligned} R &= \frac{\sigma(e^+p)}{\sigma(e^-p)} = \sqrt{\frac{N_+^+ f_+^+}{N_+^- f_+^-} \frac{N_-^+ f_-^+}{N_-^- f_-^-}} \\ &= \sqrt{R_+ R_-}, \end{aligned} \tag{9}$$

where $f_\pm^\pm$ represent unknown torus-polarity-related acceptance and detector efficiency functions. In all cases the subscript refers to the torus polarity and the superscript refers to the lepton charge. By charge symmetry, one expects $f_+^+ = f_-^-$ and $f_-^+ = f_+^-$, thus canceling out in ratio.

We checked the quality of our acceptance corrections in two ways: 1) Doing a full Monte Carlo (MC) acceptance correction, and 2) calculating the double-ratio given in Eq. 9 with no corrections at all. We found that differences in R to be smaller than the statistical uncertainty. We used the difference between our acceptance-matched results and our MC-corrected results to estimate the acceptance-related systematic uncertainty.

3.2.3. *Systematic Uncertainties*

The four major categories of systematic uncertainties that we have considered in this analysis are:

(1) **Luminosity differences between electrons and positrons.** This uncertainty was determined by a detailed MC study of the beam line that included all known lepton interactions. The MC study showed that the relative flux difference between positrons and electrons on the target was less than 0.01.
(2) **Effects of elastic event ID cuts.** This was studied by varying the widths of these cuts (from the nominal 4-σ cut to a 3-σ cut or removing the cut entirely). The differences in the final results between the nominal and the varied cuts result in an estimated absolute uncertainty of 0.0040.
(3) **Effects of fiducial cuts.** We also varied the cuts that define the good region of CLAS, again comparing the nominal results to those with the varied fiducial cuts. The estimated absolute uncertainty is 0.0071.
(4) **Acceptance effects.** As previously mentioned, this was done by comparing our nominal results (using acceptance matching) to results using a MC acceptance correction. The estimated absolute uncertainty is 0.0083 and is the largest of our systematic uncertainties.

3.3. *Early Results from CLAS*

Our final results are shown in Fig. 14 along with the previous world's data at a similar value of Q^2. A small radiative correction ($<$ 0.0049) has been applied for lepton-proton bremsstrahlung interference. There are seven previous data points in this same range of Q^2 (blue points). The plot shows a fit linear in ϵ ($R = m\epsilon + b$) that includes our data (again including point-to-point systematic uncertainties) and the blue points. The fit at this Q^2 results in an ϵ-dependence consistent with zero ($m = -0.005 \pm 0.020$) and $b = 1.028 \pm 0.017$ with $\chi^2/\nu = 0.70$. Essentially, there is no ϵ dependence at this Q^2 but there is a statistically significant deviation from unity. A constant fit of our data and the world data results in an average value of 1.024±0.0047, which is more than five standard deviations from unity, though systematic uncertainties do shrink the significance of this deviation. The figure also includes the BMT calculation.[27] There is a significant difference between our fit and the BMT calculation.

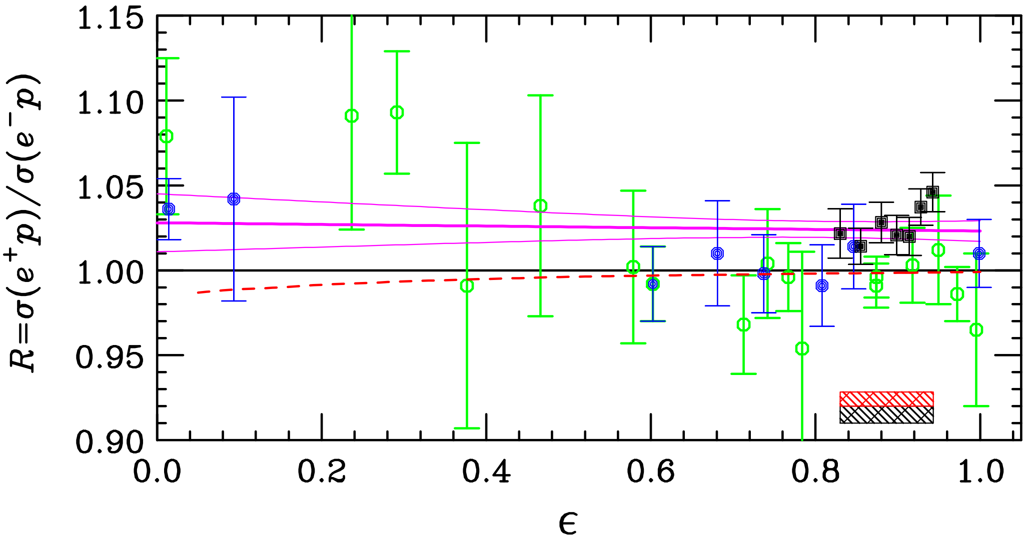

Fig. 14. Charge asymmetry ratio overlaid on the world data. Black filled squares are from this experiment at $\langle Q^2 \rangle = 0.206$ GeV^2 and have had radiative corrections applied, blue filled circles are previous world data at similar Q^2, and green hollow points the rest of the previous world data with $Q^2 < 2$ GeV^2.[28] The linear fit (heavy magenta line) includes the present data and the blue points while the light magenta lines indicate the 1σ uncertainty in the fit. The red shaded band indicates the point-to-point systematic uncertainty (1σ) and the black shaded band represents the scale-type systematic uncertainty (due to relative luminosity) on the present data. The red dashed curve is the BMT calculation[27] at $Q^2 = 0.2$ GeV^2.

4. Conclusion and Future Prospects

During late 2010 and early 2011 we conducted the full CLAS TPE experiment using an incident beam energy of 5.5 GeV and with about a 50 times higher luminosity than for the 2006 run. The final results from the experiment will have statistical uncertainties of better than 1% for $Q^2 < 1.5$ GeV^2 and better than 2% for $Q^2 < 2.5$ GeV^2 over nearly the entire ϵ range. Analysis is underway and we expect preliminary results to be available in early 2012.

There are two other experiments that will also provide measurements of the TPE effect in much the same way as the CLAS experiment. In 2009, the Novosibirsk group[33] measured $R_{2\gamma}$ at $Q^2 = 1.5$ GeV^2 and in 2012, the OLYMPUS[34] collaboration will measure $R_{2\gamma}$ at $Q^2 < 2.5$ GeV^2. Both experiments should result in similar uncertainties as our CLAS experiment though with more limited coverage in ϵ. Fig. 15 shows the expected uncertaintes and kinematic coverage once the analyses are completed.

These experiments will provide information that is vital to our understanding of the electon-scattering process as well as our understanding of the proton structure. We have heard the common mantra that "the electromagnetic probe is well understood." However, the discrepancy between Rosenbluthe and polarization measurements of the form-factor ratio indicates otherwise. Indeed, if we don't even understand elastic electron scattering, how well do we know anything we have measured with electron scattering? There are important implications for many of the nuclear physics quantities we study ranging from high-precision quasi-elastic experiments to strangeness and parity violation experiments to transition form factor exeperiments.

5. Appendix: Kinematics Definitions

Several kinematic quantities appear throughout this proceeding that require definition. Fig. 16 shows the scattering of an electron from a proton through the exchange of a single virtual photon (shown by γ^*). The incident electron is described by the four

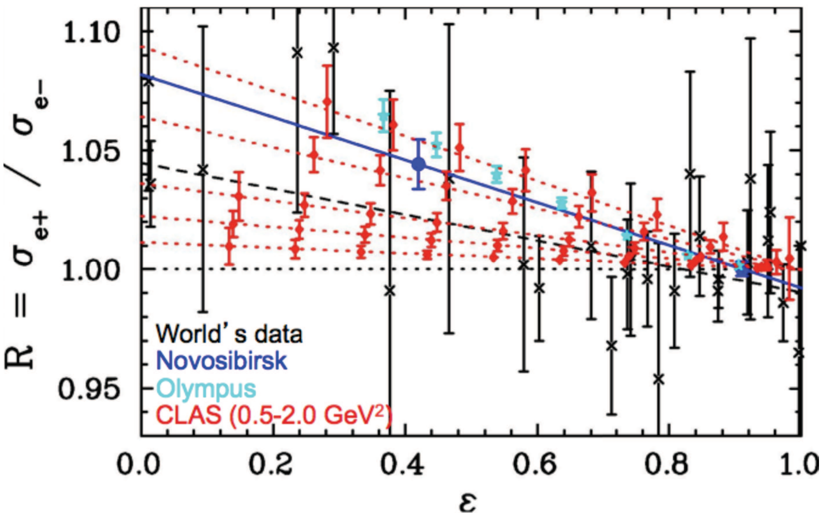

Fig. 15. Expected uncertainties and kinematic coverage for $R_{2\gamma}$ for the Novosibirsk VEPP-3 experiment (blue points), OLYMPUS (cyan points), and CLAS TPE (red points) compared to the previous world data.

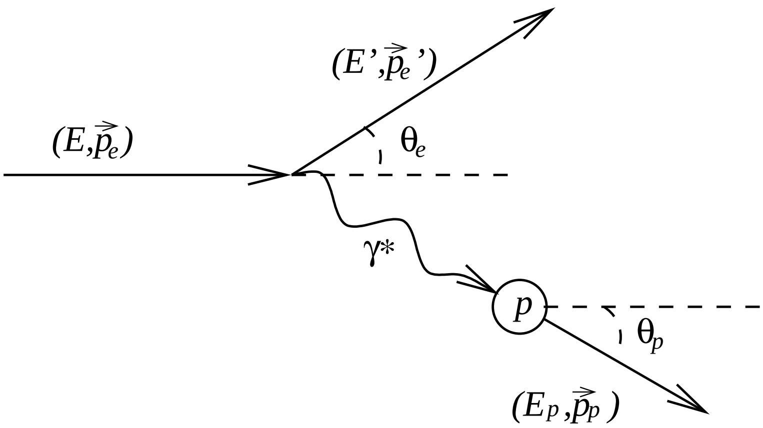

Fig. 16. Diagram of elastic scattering of an electron from a proton through the exchange of a virtual photon (γ^*).

vector $(E, \vec{p_e})$, the scattered electron by the four vector $(E, \vec{p_e}')$, and the scattered proton by the four vector $(E_p, \vec{p_p})$. The electron scattering angle is denoted by θ_e and the proton scattering angle is denoted by θ_p. A quantity that we see frequently is the square of the four-momentum transfer of the virtual photon:

$$Q^2 = -q^2 = 4EE' \sin^2 \frac{\theta_e}{2}. \tag{10}$$

This quantity can be thought of as the resolution of the virtual photon or, more appropriately for our case, how deeply the virtual photon probes the proton.

The degree of the transverse polarization of the virtual photon is given by

$$\epsilon = \left[1 + 2\left(1 + \frac{\nu^2}{Q^2}\right) \tan \frac{\theta_e}{2}\right]^{-1}, \tag{11}$$

where $\nu = E - E'$ is the energy transfer by the virtual photon.

In our expression for the cross section we also saw the term τ which is defined as

$$\tau = \frac{Q^2}{4m_p}, \tag{12}$$

where m_p is the proton mass.

Finally, the invariant mass of the intermediate hadronic state is given by

$$W = \sqrt{m_p^2 + 2m_p\nu - Q^2} = \sqrt{s}, \tag{13}$$

where s is the Mandelstam variable. In the case of elastic scattering it is always the case that $W = m_p$.

References

1. M. N. Rosenbluth, Phys. Rev. **79**, 615 (1950).
2. M. E. Christy *et al.*, Phys. Rev C**70**, 015206 (2004).
3. J. Arrington, W. Melnitchouk, and J. A. Tjon, Phys. Rev. C**76**, 035205 (2007).
4. A. I. Akhiezer and M. P. Rekalo, Sov. Phys. Dokl. **13**, 572 (1968).
5. N. Dombrey, Rev. Mod. Phys. **41**, 236 (1969).
6. A. I. Akhiezer and M. P. Rekalo, Sov. J. Part. Nucl. **3**, 277 (1974).
7. R. G. Arnold, C. E. Carlson, and F. Gross, Phys. Rev. C **23**, 363 (1981).
8. B. Milbrath *et al.*, Phys. Rev. Lett. **80**, 452 (1998); **82**, 2221(E) (1999).
9. V. Punjabi *et al.*, Phys. Rev. C **71**, 055202 (2005); M. K. Jones *et al.*, Phys. Rev. Lett. **84**, 1398 (2000).
10. O. Gayou *et al.*, Phys. Rev. C **64**, 038202 (2001).
11. M. Meziane *et al.* Phys. Rev. Lett. **106**, 132501 (2011).
12. T. Pospischil *et al.*, Eur. Phys. J. A **12**, 125 (2001).
13. O. Gayou *et al.*, Phys. Rev. Lett. **88**, 092301 (2002); Revised analysis in Ref..[18]
14. G. MacLachlan *et al.*, Nucl. Phys. **A764**, 261 (2006).
15. G. Ron *et al.*, Phys. Rev. Lett. **99**, 202002 (2007); G. Ron *et al.*, arXiv:1103.5784 [nucl-ex].
16. A. J. R. Puckett *et al.*, Phys. Rev. Lett. **104**, 242301 (2010).
17. X. Zhan *et al.*, arXiv:1102.0318 [nucl-ex].
18. A. J. R. Puckett *et al.*, arXiv:1102.5737 [nucl-ex].
19. M. K. Jones *et al.*, Phys. Rev. C **74**, 035201 (2006).
20. C. B. Crawford *et al.*, Phys. Rev. Lett. **98**, 052301 (2007).
21. R. C. Walker *et al.*, Phys. Rev. D **49**,5671 (1994).
22. L. Andivahis *et al.*, Phys. Rev. D **50**, 5491 (1994).
23. L. A. Qattan *et al.*, Phys. Rev. Lett. **94**, 142301 (2005).
24. Y. S. Tsai, Phys. Rev. **122**, 1898 (1961); L. W. Mo and Y. S. Tsai, Rev. Mod. Phys. **41**, 205 (1969).
25. L. C. Maximon and J. A. Tjon, Phys. Rev. C **62**, 054320 (2000).
26. J. Arrington, P. G. Blunden, and W. Melnitchouk, arXiv:1105.0951 [nuclt-th] (2011).
27. P. G. Blunden, W. Melnitchouk, and J. A. Tjon, Phys. Rev. C **72**, 034612 (2005).
28. J. Arrington, Phys. Rev. C **69**, 032201 (2004).
29. D. Yount and J. Pine, Phys. Rev. **128**, 1842 (1962).
30. Jefferson Lab Experiment E07-005, *Beyond the Born approximation: A precise comparison of positron-proton and electron-proton elastic scattering in CLAS*, A. Afanasev *et al.*, spokespersons.
31. B. A. Mecking *et al.*, Nucl. Instr. and Meth. A **503**, 513 (2003).
32. D. I. Sober *et al.*, Nucl. Instr. and Meth. A **440**, 263 (2000).
33. J. Arrington *et al.*, VEPP-3 proposal, arXiv:nucl-ex/040802, (2004).
34. M. Kohl, API Conf. Proc. 1160, 19 (2009).